Multifunctional cantilever-free scanning probe arrays coated with multilayer graphene

Shim, W.; Zhou, X.; Rasin, B.; Liao, X.; Brown, Keith A.; Mirkin, Chad A.

2012

Shim, W., Brown, K. A., Zhou, X., Rasin, B., Liao, X., & Mirkin, C. A. (2012). Multifunctional cantilever-free scanning probe arrays coated with multilayer graphene. Proceedings of the national academy of sciences, 109(45), 18312-18317.

https://hdl.handle.net/10356/98253

https://doi.org/10.1073/pnas.1216183109

Multifunctional cantilever-free scanning probe arrays coated with multilayer graphene

Wooyoung Shim[a,b,1], Keith A. Brown[b,c,1], Xiaozhu Zhou[b,c,d], Boris Rasin[a,c], Xing Liao[a,c], and Chad A. Mirkin[a,b,c,2]

[a]Department of Materials Science and Engineering, [b]Department of Chemistry, and [c]International Institute for Nanotechnology, Northwestern University, Evanston, IL 60208; and [d]School of Materials Science and Engineering, Nanyang Technological University, Singapore 639798

Contributed by Chad A. Mirkin, September 27, 2012 (sent for review August 8, 2012)

Scanning probe instruments have expanded beyond their traditional role as imaging or "reading" tools and are now routinely used for "writing." Although a variety of scanning probe lithography techniques are available, each one imposes different requirements on the types of probes that must be used. Additionally, throughput is a major concern for serial writing techniques, so for a scanning probe lithography technique to become widely applied, there needs to be a reasonable path toward a scalable architecture. Here, we use a multilayer graphene coating method to create multifunctional massively parallel probe arrays that have wear-resistant tips of uncompromised sharpness and high electrical and thermal conductivities. The optical transparency and mechanical flexibility of graphene allow this procedure to be used for coating exceptionally large, cantilever-free arrays that can pattern with electrochemical desorption and thermal, in addition to conventional, dip-pen nanolithography.

scanning probe microscopy | tip modification | energy delivery | tip wear | friction

The ability to prepare nanoscale structures with the tip of a scanning probe has stimulated intense research efforts to use the scanning probe microscope as an instrument for nanofabrication on surfaces with high resolution, registration accuracy, and relatively low cost. These techniques rely on specific probes to enable the transfer of materials or energy from the probe to a surface: Dip-pen nanolithography (DPN) requires tips with controlled hydrophobicitiy (1–3); anodic oxidation requires electrically conductive tips (4, 5); mechanical scratching or nanografting requires rigid, wear-resistant tips (6–8); and thermal-scanning probe lithography (SPL) requires tips with integrated heaters (9). Therefore, understanding the tradeoffs inherent in using specialized SPL probes is important, especially when considering high throughput SPL techniques. A challenge common to all SPL techniques is to pattern with high throughput despite the serial nature of probe-based lithography. This has been addressed by the development of specialized systems, for example, one- (10) and two-dimensional cantilever arrays (11, 12). The recent development of cantilever-free arrays provides a low-cost alternative to cantilever arrays for parallel SPL (13, 14).

Recently, hard-tip, soft-spring lithography (HSL) has emerged as a technique for patterning sub-50-nm features over centimeter scales (15) by using an array of silicon tips resting on a compliant polydimethylsiloxane (PDMS) layer. These arrays are well suited for printing organic and inorganic structures in a high throughput and combinatorial fashion, but the versatility of these arrays is limited by the low electrical and thermal conductivities of PDMS. The adaptation of the cantilever-free architecture to additional SPL modalities would be powerful, but only low-temperature processing steps that do not compromise the transparency and compliance of the PDMS layer can be considered. Considerable research has focused on improving the capabilities of conventional SPL tips through thin-film coating, but these modifications can blunt the tips significantly (16). Furthermore, metal coatings that are used to improve the electrical conductivity (17) are opaque and susceptible to tip wear, whereas wear-resistant coatings such as diamond are electrically insulating (16). Graphene is a promising candidate material for a multifunctional coating because of its high electrical and thermal conductivities, optical transparency, low friction, and mechanical strength (18). Recently, metal-coated probes have been used for the catalytic growth of graphene for applications in molecular electronics, but this technique requires a thick metal coating, annealing at 950 °C, and does not result in uniform probe coating (19).

Herein, we describe a simple strategy for coating HSL tip arrays with multilayer graphene to generate tips that are highly wear-resistant and electrically and thermally conducting, in a way that preserves the optical transparency of the array and the sharpness of the tips. To illustrate the versatility of graphene-coated HSL tip arrays, we have performed patterning with two techniques that would not be possible without graphene-coated arrays: (*i*) electrochemical desorption and (*ii*) thermal-DPN. Additionally, we show that graphene coating results in a 40% reduction in tip-sample friction, compared with silicon tips, which leads to substantially decreased wear. The simplicity and versatility of this graphene-coating technique make it valuable to the scanning probe lithography, nanofabrication, and microscopy communities.

Results and Discussion

The key innovation that enables graphene-coated HSL tip arrays is a simple protocol to conformally coat the surface of an HSL tip array with multilayer graphene (Fig. 1*A*). In a typical experiment, 1×1 cm^2 HSL tip arrays with 4,489 (67×67) tips and a tip-to-tip pitch of 150 μm were fabricated according to literature methods (15). Chemical-vapor–deposited, large-area, multilayer graphene films on Ni (Graphene Laboratories Inc.) were spin-coated with a ~70-nm-thick poly(methylmethacrylate) (PMMA) layer for support (*SI Appendix*, Fig. S1). Following etching of the Ni film, the separated PMMA/graphene film was transferred onto an HSL tip array (1×1 cm^2) that had been pretreated with oxygen plasma (Fig. 1*B*). The transfer took place while the PMMA/graphene layer was floating on a mixture of water and ethanol (1:2, vol/vol). The HSL tip array was submerged in the liquid and held at an angle of ~40° with respect to the surface. The solvent was then allowed to evaporate, which caused the PMMA/graphene to fall onto the tip array and coat it conformally (Fig. 1*C*). Tilting the array during the solvent evaporation process significantly improved the coverage of graphene onto the tip array (*SI Appendix*, Fig. S2), and using a mixture of water and ethanol reduced the surface tension and improved the conformal coating (*SI Appendix*, Fig. S3). Subsequent washing with acetone was

Author contributions: W.S., K.A.B., and C.A.M. designed research; W.S., K.A.B., X.Z., B.R., and X.L. performed research; W.S., K.A.B., X.Z., B.R., X.L., and C.A.M. analyzed data; and W.S., K.A.B., and C.A.M. wrote the paper.

The authors declare no conflict of interest.

[1]W.S. and K.A.B. contributed equally to this work.

[2]To whom correspondence should be addressed. E-mail: chadnano@northwestern.edu.

This article contains supporting information online at www.pnas.org/lookup/suppl/doi:10.1073/pnas.1216183109/-/DCSupplemental.

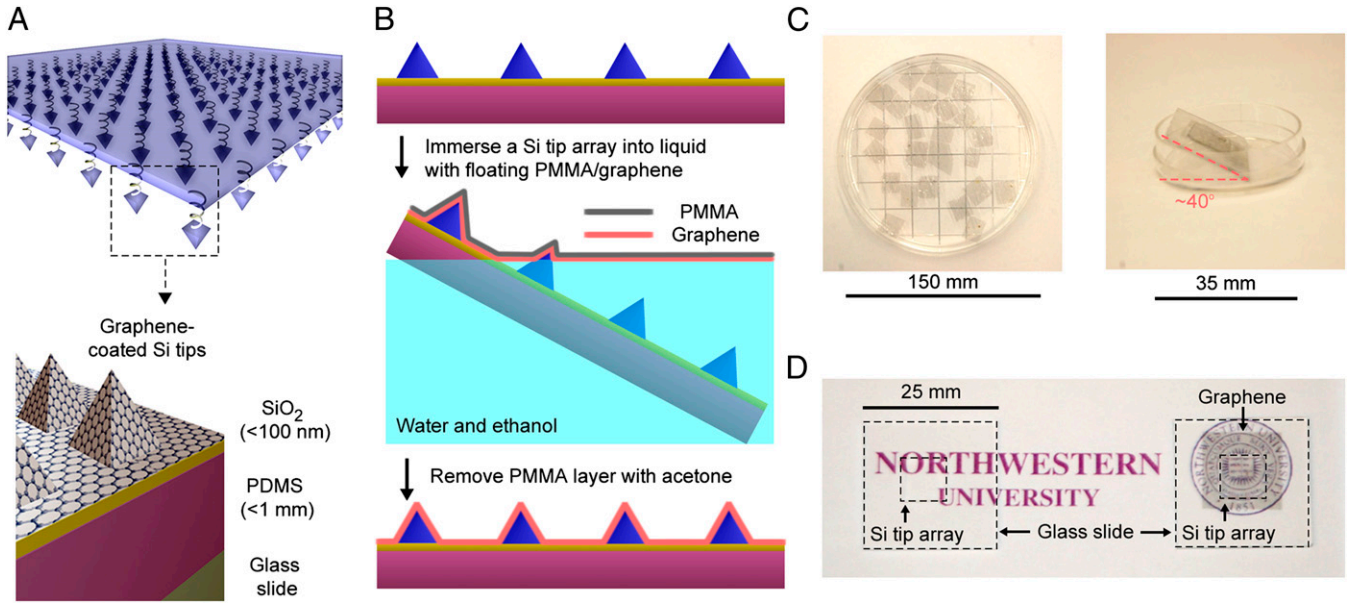

Fig. 1. Fabrication of graphene-coated HSL tip arrays. (*A*) Illustration of a multilayer graphene-coated hard-tip, soft-spring lithography (HSL) tip array supported by a transparent, soft backing layer that provides mechanical compliance to each tip. Schematic of the architecture of a graphene-coated HSL tip array (*Lower*). (*B*) Experimental protocol used to fabricate graphene-coated HSL tip arrays. (*C*) PMMA/graphene layers floating on water before coating. Transfer of PMMA/graphene onto an HSL tip array by tilting the array and evaporating the solvent in air, resulting in a conformally graphene-coated HSL tip array. (*D*) The transparency of an uncoated HSL tip array (*Left*) is compared with a graphene-coated HSL tip array (*Right*).

used to remove the PMMA. Due to the high adhesion energy of graphene relative to its bending energy (20), the graphene established conformal coverage of the tip surface (*SI Appendix*, Fig. S4). The graphene-coated, glass/PDMS-supported tip arrays remained transparent (Fig. 1*D*), which allowed for optical leveling of the tips with respect to a surface.

To evaluate the uniform and conformal graphene coating of HSL tip arrays, scanning electron microscopy (SEM) and Raman spectroscopy were performed. Before graphene coating, the HSL tip array exhibited a smooth and uniform elastomer surface (Fig. 2*A*). After coating with PMMA/graphene, folds and creases were visible on the surface of the elastomer (Fig. 2*B*). When the PMMA was removed, the surface appeared cleaner, but folds remained visible, providing evidence for the presence of graphene (Fig. 2*C*). There was no significant change in the tip height throughout the coating process, but the tip diameter increased from 23 ± 3 nm to 40 ± 5 nm after graphene coating, an increase commensurate with the measured ~9-nm thickness of the 10- to 20-layer graphene film (*SI Appendix*, Fig. S5). Optical microscopy confirmed the presence of PMMA/graphene on the surface of the HSL tip array; one could easily see a network of folds that formed a regular lattice with vertices defined by the tips (Fig. 2*D*). Note that "tenting" is not observed and the folding provides additional flexibility when the PDMS supporting the tips is compressed during writing. After the PMMA was removed in acetone, the folds were still and were visualized by atomic force microscopy (Fig. 2*D*). Raman spectroscopy (532-nm excitation) was used to provide direct evidence for the presence of graphene at the tips of the probes in the HSL tip array. Raman mapping of the Si band (499–546 cm^{-1}) clearly depicts the form of a single Si tip resting on a flat SiO_2 surface (Fig. 2*E Upper*). Mapping of the graphene G band (1,569–1,614 cm^{-1}) in the same region shows the triangular shape of the tip as well as a flat supporting backing layer (Fig. 2*E Lower*). The colocalization of the Si and graphene bands provides evidence for the conformal coating of graphene layers onto the HSL tip array. Furthermore, a spectrum taken on the tip shows a broad 2D band, and more intense G band, $I(G) > I(2D)$, which is characteristic of multiple graphene layers (21, 22) (Fig. 2*F*).

The graphene coating of the tip array transforms HSL from a technique limited to DPN (1) and nanografting (7) to one capable of lithographic methods that require probes with high electrical conductivity. For example, electrical contact can be readily made with regions of the graphene film extending beyond the tip array (Fig. 3*A*). Electrical contact was verified by measuring a current that flows through the tips and into the substrate when the tip array is in contact with the surface (*SI Appendix*, Fig. S6). The ability of a graphene-coated HSL tip array to conduct electricity, in principle, allows one to use an electric field and HSL to electrochemically desorb an alkanethiol self-assembled monolayer (SAM) from an Au surface (23–27). To evaluate the prospects for electrochemical desorption, SAMs were prepared by soaking an Au-coated silicon wafer in an ethanol solution of 16-mercaptohexadecanoic acid (MHA, 1 mM) for 1 h followed by copious rinsing with ethanol and drying under N_2. A negative bias voltage was applied to the graphene-coated HSL tip arrays with respect to the SAM-modified Au surface (Fig. 3*B*). To investigate the effect of tip voltage on feature size, the tip array was used to pattern a square lattice of points with a constant dwell time of 10 s while the tip bias voltage was varied from −7 to −18 V (Fig. 3*C*). Following patterning, the surface was chemically etched to remove the Au in patterned regions where there was no longer a protective SAM. Recessed areas, which correspond to patterned spots, are observed, and the average feature diameter exhibits an exponential dependence on reductive potential (*SI Appendix*, Fig. S7). These observations are consistent with a kinetic model for the reductive desorption of an alkanethiol SAM (28). To evaluate the ability of this method to generate smaller features, the tip-surface contact time was reduced to 5 s with a voltage of −5 V. Features made in this process exhibit an average feature diameter of 98 ± 7 nm (Fig. 3*D*). The ability to generate arbitrary patterns with graphene-coated HSL tip arrays was demonstrated by reproducing a dot array (*SI Appendix*, Fig. S8) depicting a portion of the constellations in the northern hemisphere. In this proof-of-

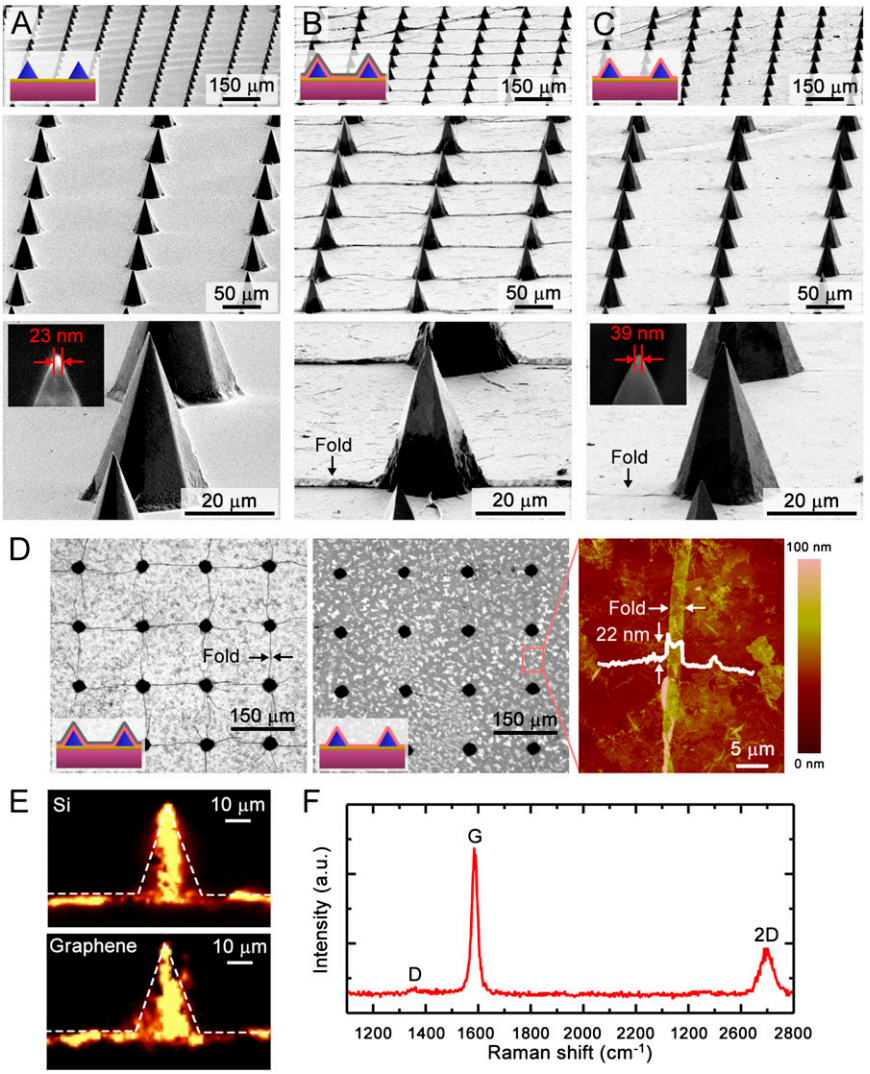

Fig. 2. Characterization of graphene-coated HSL tip arrays. Scanning electron microscopy (SEM) images of an HSL tip array (*A*) before graphene coating, (*B*) after coating with PMMA/graphene, and (*C*) after removal of the PMMA. (*D*) Top-view optical images of graphene folds between tips before and after removal of the PMMA. After the PMMA was removed, the existence of graphene folds was confirmed by a topographical image taken by atomic force microscopy. (*E*) Raman mapping of the Si band (499–546 cm^{-1}, *Upper*) and the graphene G band (1,569–1,614 cm^{-1}, *Lower*). The overlap of these maps confirms coverage of the silicon tip with graphene. (*F*) Raman spectra (excitation wavelength $\lambda = 532$ nm) for graphene layers on a Si tip shown in *E*.

concept experiment, the resulting etched Au pattern generated by each of the 4,489 tips in the 1×1 cm^2 array is an accurate miniaturized duplication (80×100 μm^2) of the bitmap image with an average dot diameter of 590 ± 60 nm (Fig. 3*E*).

The presence of a conducting graphene layer coating, not only on the tips but also on the base of the HSL tip array, allows one to apply a potential and drive an electrical current across the array, which can be used to locally heat the tips through resistive heating. This heating effect was initially evaluated in the context of lithography by exploring the ability of graphene-coated HSL tip arrays to deposit a polymer mask via thermal-DPN (2) (Fig. 4*A*). In a typical experiment, drop casting of a photoresist (S1805; Shipley) was used to coat the tip array followed by solvent evaporation for 30 min at room temperature. This resist was chosen because of its relatively low glass transition temperature (~60 °C) (29) and widespread use in semiconductor processing. Because the photoresist is a glass at room temperature, when the tip array was pressed against a silicon surface, no material was transferred to the surface. In contrast, when it was pressed against the surface while 15 mW of electrical power was applied to the tip array, the resist uniformly transferred to the substrate. As proof-of-concept, using a graphene-coated HSL tip array consisting of 4,489 tips, we created dot patterns on Si wafers coated with 15 nm of SiO_2. The pattern covers 1 cm^2 and consists of over 11 million dot features, with each tip responsible for making a 51×51 array of dots (based upon a contact time of 1 s and a relative humidity of 30%). Importantly, the polymer pattern can be transferred into the SiO_2 substrate by etching with ammonium fluoride (20% NH_4F; Time Etch; Transene) (Fig. 4*A*). The resulting average feature size was determined by SEM to be 80 ± 9 nm, and the arbitrary patterning capability of this technique was further demonstrated by generating 4,489 duplicates of a pattern depicting constellations (Fig. 4*C*; for complete bitmap image see *SI Appendix*, Fig. S9). The average feature diameter was determined by atomic force microscopy (AFM) to be 170 ± 20 nm.

Because a relatively low applied power was necessary to achieve thermal transport, measurements of the temperature coefficient of resistance were performed to estimate the average temperature of the graphene film. To examine how the electrical resistance

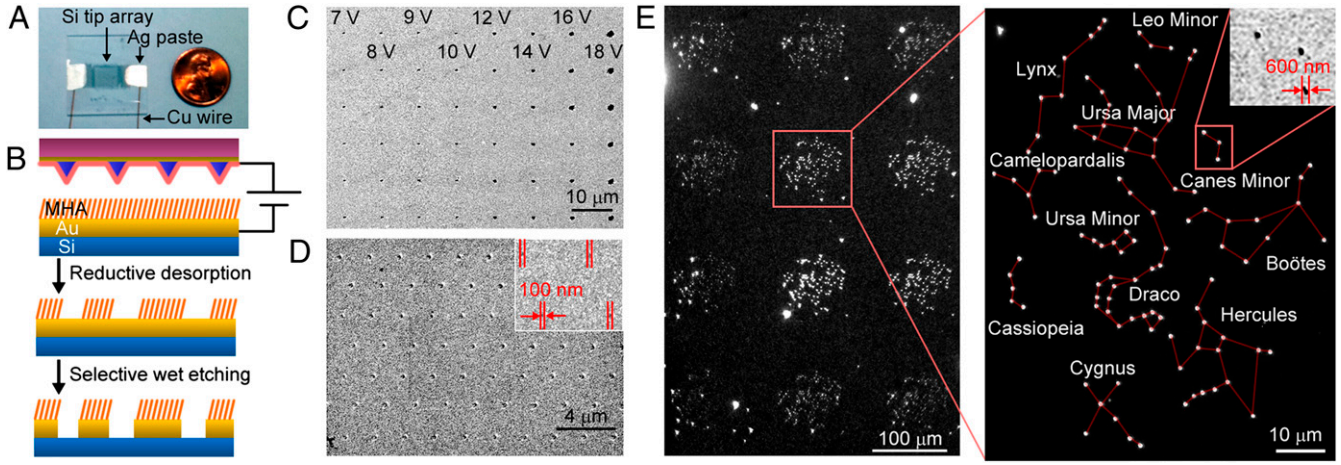

Fig. 3. Electrochemical patterning with graphene-coated HSL tip arrays. (*A*) Optical image of a graphene-coated HSL tip array that has been electrically contacted on two sides of the array. (*B*) A schematic illustration of the electrochemical desorption of 16-mercaptohexadecanoic acid (MHA) features by coming into contact with a surface while maintaining a voltage bias with respect to a surface followed by Au removal by wet etching. (*C*) SEM image of a pattern of etched Au holes of different sizes created by varying the bias voltage from −7 to −18 V while patterning spots for 10 s. (*D*) SEM image of a pattern of etched Au holes with a contact time of 5 s and at a reductive potential of −5 V. (*E*) SEM image of arbitrary Au hole patterns written over a large scale consisting of arrays of constellations in the northern hemisphere including Draco, Hercules, and Ursa Major, written with a bias voltage of −10 V, a contact time of 10 s, and a relative humidity of 30%. The right image shows a magnified image of the pattern written by a single probe with guide lines depicting the constellations. The inset shows a magnified SEM image of a highlighted area.

of the graphene film changes with temperature, the resistance of the graphene was measured while the temperature of the graphene-coated HSL tip array was adjusted on a hot plate. This provides a measure of the temperature coefficient of resistance κ, which was determined to be -3×10^{-3}/K (*SI Appendix*, Fig. S10), in good agreement with previous reports (30). The temperature in the graphene film was then estimated by recording the change in resistance ΔR of the graphene resistor as a function of applied power (*SI Appendix*, Fig. S10). For example, when 24 mW of power was applied to a 1-cm^2 graphene-coated HSL tip array, $\Delta R/R = -0.18$, which corresponds to $\Delta T = 58$ °C when converted using κ. This large temperature change in response to modest applied power is attributed to the graphene resistor being sandwiched between thermally insulating SiO_2/PDMS and photoresist layers, localizing the heat generation to the graphene.

Graphene and graphite are widely studied as lubricating materials (31), so the graphene-coating technique presented here has the potential to reduce tip-sample friction and therefore tip wear. To test this hypothesis, the tip-sample friction was quantitatively measured using friction force microscopy. Because a cantilever is needed to quantitatively evaluate tip-sample friction, conventional contact mode atomic force probes (PPP-CONT; NanoWorld AG) were coated with graphene using the same protocol implemented for preparing the graphene-coated HSL tip arrays (*SI Appendix*, Fig. S11). The contact mode probes were chosen because of the similarity between their tips and those in HSL tip arrays. Both are composed of silicon and fabricated with a self-sharpening anisotropic etch. The commercial probes are slightly sharper owing to an additional sharpening process, having a radius of curvature <7 nm, whereas HSL tip arrays have an ∼11-nm radius of curvature. The coefficient of friction between the tip and the surface was estimated using a wedge calibration technique (32). Graphene-coated and uncoated probes were scanned across the flat surface of a Si(100) wafer and angled Si(111) planes exposed by anisotropic etching (topography, Fig. 5*A*). Measurement on surfaces with different, but known, angles is necessary to remove the influence of imperfect alignment of the tip (32). Therefore, the lateral force on both probes was measured in three distinct topographical regions

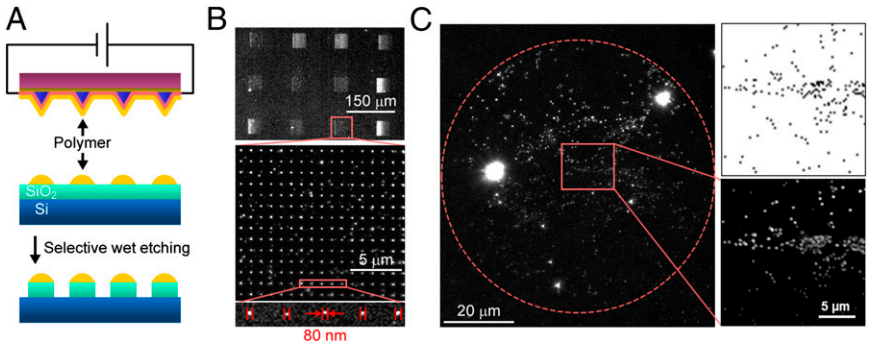

Fig. 4. Thermal patterning with graphene-coated HSL tip arrays. (*A*) A schematic illustration of the selective patterning of a polymer resist by resistive heating of a graphene-coated HSL tip array followed by SiO_2 removal by wet etching. (*B*) A dark field optical image of square arrays of photoresist dots patterned on an SiO_2/Si surface created by heating the graphene-coated tip array with 15 mW. A magnified SEM image of a dot array depicting 80-nm-diameter features (*Lower*). (*C*) A dark field optical image of a (100 × 100 μm^2) patterned dot pattern consisting of 1,088 dots corresponding to a star field. These patterns were generated with an applied power of 23 mW, a dwell time of 1s, and patterning at 30% relative humidity. A magnified dark field optical image (*Lower Right*) is compared with a section of the source pattern (*Upper Right*).

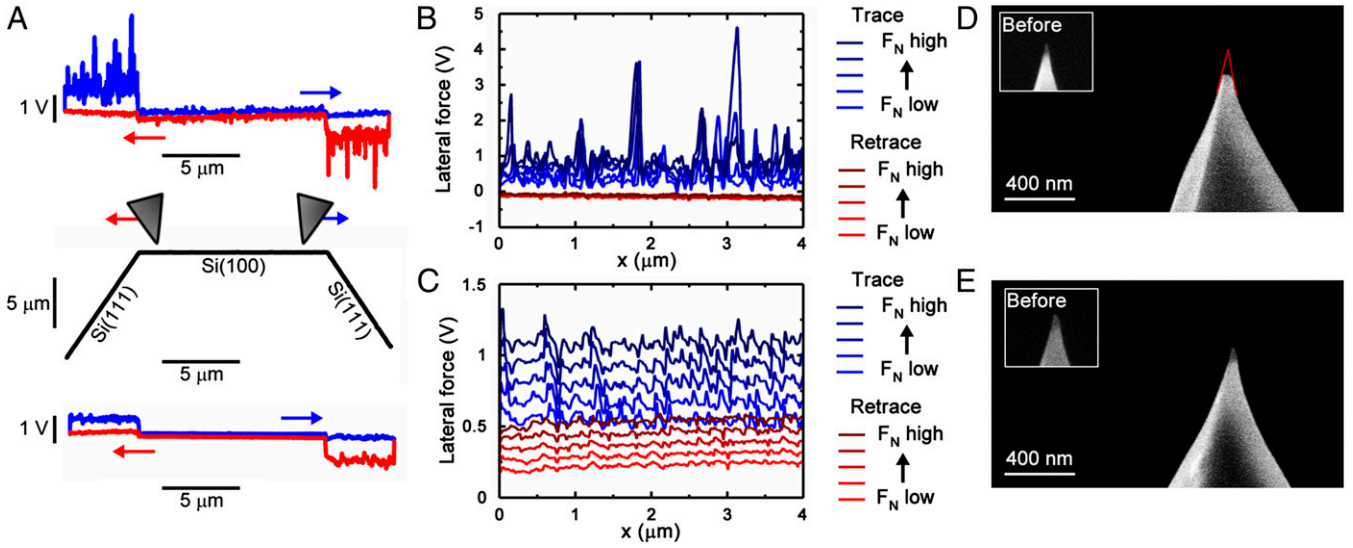

Fig. 5. Mechanical properties of graphene-coated Si tips. (*A*) Lateral force and topography (*Middle*) measured for a Si tip (*Top*) and a Si tip that has been coated in graphene (*Bottom*) as they are scanned across a Si surface consisting of a flat (100) and two sloped (111) facets. The lateral force measured from the (*B*) Si tip and (*C*) graphene-coated Si tip under an applied load increasing from ~100 to ~300 nN. SEM images of a (*D*) Si tip and (*E*) graphene-coated Si tip after 500 μm of scanning in contact with a Si surface with an applied load of 50 nN. The insets show the tips as imaged before the wear experiments at the same magnification. The red outline above the Si probe depicts the profile before the wear experiment.

(Fig. 5*A*). A qualitative difference between the probes is immediately apparent: many peaks corresponding to stick-slip events are visible in the lateral force data for the uncoated probe, whereas the lateral force measured with the graphene-coated probe displays much smaller stick-slip events and is markedly smoother (compare upper and lower scans in Fig. 5*A*). To estimate this improvement in friction performance, we calculated the standard deviation of each friction force curve fit to a piecewise series of lines corresponding to the three topographical regions. Through this analysis, deviations in the friction force curves from graphene-coated probes were found to be ~20% the magnitude of those observed for uncoated probes. We repeated this measurement for a series of normal forces ranging from 100 to 300 nN (Fig. 5 *B* and *C*). By examining how the offset and width of each friction loop changes with applied load, the coefficient of friction was determined for an uncoated probe on the Si(111) face to be 0.35, in agreement with previous reports (32). In contrast, the two measured graphene-coated probes exhibited coefficients of friction of 0.22 and 0.23, showing a ~35% reduction from the uncoated probe (*SI Appendix*, Fig. S12). It is worth emphasizing that these measurements depend highly on dynamic conditions such as relative humidity (33), tip wear (34), and the condition of the surface. In addition, the measured coefficients of friction required scanning a distance of 10 mm to stabilize for all probes measured (*SI Appendix*, Fig. S12), which we attribute to the high tip-sample forces used in this measurement, which changed conditions on the tip and surface.

To supplement the aforementioned measurements of tip-sample friction, and also directly visualize tip wear, a less destructive systematic measurement of friction was performed in conjunction with SEM analysis of tip wear. To create a baseline for wear studies, SEM imaging of six uncoated and four graphene-coated probes was performed (Fig. 5 *D* and *E*). The probes were then calibrated by measuring force–distance curves followed by thermal tuning to determine their spring constants and deflection sensitivities. They were then scanned in contact mode on a smooth Si(100) surface over a distance of 500 μm at 1 μm/s with 50 nN of applied force. The lateral deflection d of each AFM probe per unit of normal force (the sum of adhesion force and applied normal force) was used to estimate the friction experienced by each probe. We find a 40% reduction in lateral deflection for graphene-coated probes ($d = 0.91 \pm 0.05$ mV/nN) compared with uncoated ones ($d = 1.5 \pm 0.2$ mV/nN). This result is consistent with the wedge calibration results presented above. Following scanning, the probes were imaged again in the SEM. The graphene-coated tip exhibited barely any wear, whereas the uncoated probe was blunted considerably (Fig. 5 *D* and *E*). Therefore, these results suggest that the reduction in tip-sample friction from graphene coating could improve the wear performance of atomic force microscope probes.

We have outlined a simple procedure for coating scanning probes with multilayer graphene films that offers significantly improved versatility and performance. The nanometer thickness, transparency, electrical conductivity, and lubricating properties of graphene make it a powerful addition to a scanning probe. Given the simplicity of this technique, especially compared with conventional methods of metal coating, it is conceivable that graphene-coated probes could be widely applied in both lithography and imaging applications. In particular, HSL with graphene-coated arrays is a powerful nanopatterning system that can achieve both large-area patterning and high resolution, and hence is a significant step toward the realization of true benchtop nanofabrication.

Materials and Methods

Graphene Transfer onto an HSL Tip Array. Ten- to 20-layer graphene grown on Ni/Si surfaces (Graphene Laboratories Inc.) was used for all experiments. The as-grown graphene film on a 4-inch Ni/Si wafer was spin-coated with PMMA polymer (495 A2; MicroChem Corp.) at 500 rpm for 10 s with a ramping speed of 100 rpm/s followed by 5,000 rpm, 60 s with a ramping speed of 1,000 rpm/s). The sample was allowed to harden at room temperature for 24 h. The PMMA thickness measured by AFM was ~70 nm. The wafer was then cut into 1×1 cm^2 pieces and immersed into an aqueous iron chloride solution (reagent grade, 97%, 157740, CAS no. 0007705–08-0; Sigma-Aldrich) at a concentration of 1 M (50 g of $FeCl_3$ and 308 mL of deionized water) for 24 h at room temperature. The separated PMMA/graphene layer was rinsed with deionized water and then transferred onto an HSL tip array that had been oxygen-plasma–treated for 2 min at ~100 mTorr with 30 W. The transfer process took place by submerging the HSL tip array in an ethanol/water mixture (2:1) and resting it at a tilt of ~40° with respect to the liquid surface. The fluid was then allowed to evaporate over the course of ~48 h. Tilting the array during this process helped to coat the array in a row-by-row fashion,

and thus significantly enhanced the coverage of graphene on the tip array. Finally, the graphene-coated HSL tip array was soaked in acetone for 2 h and then rinsed in ethanol to remove the PMMA.

Electrically Conductive HSL for Patterning. SAMs of MHA were prepared on electron-beam evaporated Au thin films (25 nm Au on 5 nm Ti) by immersing the substrate in a solution of 1 mM MHA in ethanol for 1 h, followed by rinsing with ethanol, rinsing with deionized water, and drying with nitrogen. A graphene-coated HSL tip array was mounted in an XE-150 scanning probe platform (Park Systems) and attached to a source meter (2400-C Source Meter; Keithley) to provide a voltage bias. The graphene-coated HSL tip array was held at a bias voltage between –5 V and –20 V while the surface was grounded. To perform lithography, the tip array was brought into contact with the MHA SAM in a series of points to selectively desorb portions of the MHA SAM surface under ambient conditions (~30% humidity, 23 °C). To make the patterned features easier to visualize, wet etching was performed to remove the gold no longer protected by the MHA SAM. The resulting recessed features were characterized with optical microscopy (Zeiss) and SEM (S4800; Hitachi).

Thermally Conductive HSL for Patterning. To generate patterns with thermal-DPN, photoresist (S1805; Shipley) was drop-coated onto a graphene-coated HSL tip array. The photoresist was allowed to dry at room temperature for 30 min. The graphene-coated HSL tip array was electrically contacted by silver paste on opposing sides of the array and connected to a voltage supply (triple output DC power supply; B&K Precision Corp.). The voltage (179 True RMS Multimeter; Fluke) and current (34401A 6 1/2 Digit Multimeter; Agilent) were monitored to calculate the resistance of the graphene during heating. By applying a voltage across the graphene, the resistance was observed to decrease as local resistive heating occurred. Typically, an applied power of 23 mW was used for a 1×1 cm^2 tip array. Photoresist was thermally transferred to a PVD-grown SiO_2 (15 nm)/Si surface (~30% humidity, 23 °C). The patterned sample was etched (Timetch; Transene) to transfer the photoresist patterns onto SiO_2. The resulting features were characterized with optical microscopy (Zeiss), SEM (S4800; Hitachi), and AFM (Dimension Icon; Bruker).

Friction Force Microscopy. Quantitative friction force microscopy was performed in a Bruker Dimension Icon atomic force microscope. Both uncoated and graphene-coated probes (PPP-CONT; NanoWorld AG) were mounted in the probe holder with special care to keep the cantilever parallel to the probe holder. Next, the deflection sensitivity (200 nm/V typical) of the probes was found by taking three force–distance curves and finding the average slope of the approach line. These force–distance curves were also used to calculate the average tip-sample adhesion force. Next, the spring constant (0.3 N/m typical) was found through thermal calibration. The probes were then scanned across the flat surface of a Si(100) wafer with square pyramidal holes prepared by KOH etching to produce Si(111) faces at a known angle. Scan regions are 20×1 μm^2 at a resolution of $2{,}048 \times 8$ pixels and scanned at 4 μm/s. Proportional gain was set to 0 with integral gain of 5 to remove the possibility of underdamped feedback reducing the tip-sample friction (32). This region was rescanned while sweeping the applied force from ~100 to ~300 nN. The change of the width and offset of each friction loop with respect to applied force was used to extract the coefficient of friction following Varenberg et al. (32). The process of varying the applied force was repeated 10 times for each probe to examine change in the tip-sample friction as the probe continued to scan the surface. Experiments were performed at room temperature (22 °C) in low ambient humidity (RH ~33%).

ACKNOWLEDGMENTS. This material is based upon work supported by Defense Advanced Research Projects Agency/Microsystems Technology Office Award N66001-08-1-2044; Asian Office of Aerospace Research and Development Award FA2386-10-1-4065; Air Force Office of Scientific Research Awards FA9550-12-1-0280 and FA9550-12-1-0141; National Science Foundation Awards DMI-1152139 and DMB-1124131; Department of Defense/Naval Postgraduate School/National Security Science and Engineering Faculty Fellowship Awards N00244-09-1-0012 and N00244-09-1-0071; Chicago Biomedical Consortium with support from Searle Funds at The Chicago Community Trust; and Centers of Cancer Nanotechnology Excellence initiative of the National Institutes of Health Award U54 CA151880. K.A.B. and X.L. acknowledge support from Northwestern University's International Institute for Nanotechnology.

1. Piner RD, Zhu J, Xu F, Hong SH, Mirkin CA (1999) "Dip-Pen" nanolithography. *Science* 283(5402):661–663.
2. Salaita K, Wang Y, Mirkin CA (2007) Applications of dip-pen nanolithography. *Nat Nanotechnol* 2(3):145–155.
3. Braunschweig AB, Huo F, Mirkin CA (2009) Molecular printing. *Nat Chem* 1(5): 353–358.
4. Snow ES, Campbell PM (1994) Fabrication of Si nanostructures with an atomic force microscope. *Appl Phys Lett* 64(15):1932–1934.
5. Snow ES, Campbell PM (1995) AFM fabrication of sub-10-nanometer metal-oxide devices with in situ control of electrical properties. *Science* 270(5242):1639–1641.
6. Kim Y, Lieber CM (1992) Machining oxide thin films with an atomic force microscope: pattern and object formation on the nanometer scale. *Science* 257(5068):375–377.
7. Xu S, Miller S, Laibinis PE, Liu G (1999) Fabrication of nanometer scale patterns within self-assembled monolayers by nanografting. *Langmuir* 15(21):7244–7251.
8. Bhaskaran H, et al. (2010) Ultralow nanoscale wear through atom-by-atom attrition in silicon-containing diamond-like carbon. *Nat Nanotechnol* 5(3):181–185.
9. Mamin HJ, Rugar D (1992) Thermomechanical writing with an atomic force microscope tip. *Appl Phys Lett* 61(8):1003–1005.
10. Hong S, Mirkin CA (2000) A nanoplotter with both parallel and serial writing capabilities. *Science* 288(5472):1808–1811.
11. Salaita K, et al. (2006) Massively parallel dip-pen nanolithography with 55000-pen two-dimensional arrays. *Angew Chem Int Ed* 45(43):7220–7223.
12. Vettiger P, et al. (2000) The 'Millipede'—More than one thousand tips for future AFM data storage. *IBM J Res Develop* 44(3):323–340.
13. Huo F, et al. (2008) Polymer pen lithography. *Science* 321(5896):1658–1660.
14. Giam LR, et al. (2012) Scanning probe-enabled nanocombinatorics define the relationship between fibronectin feature size and stem cell fate. *Proc Natl Acad Sci USA* 109(12):4377–4382.
15. Shim W, et al. (2011) Hard-tip, soft-spring lithography. *Nature* 469(7331):516–520.
16. Liu J, et al. (2010) Preventing nanoscale wear of atomic force microscopy tips through the use of monolithic ultrananocrystalline diamond probes. *Small* 6(10):1140–1149.
17. Vasko SE, et al. (2011) Serial and parallel Si, Ge, and SiGe direct-write with scanning probes and conducting stamps. *Nano Lett* 11(6):2386–2389.
18. Geim AK (2009) Graphene: Status and prospects. *Science* 324(5934):1530–1534.
19. Wen Y, et al. (2012) Multilayer graphene-coated atomic force microscopy tips for molecular junctions. *Adv Mater (Deerfield Beach Fla)* 24(26):3482–3485.
20. Koenig SP, Boddeti NG, Dunn ML, Bunch JS (2011) Ultrastrong adhesion of graphene membranes. *Nat Nanotechnol* 6(9):543–546.
21. Shih CJ, et al. (2011) Bi- and trilayer graphene solutions. *Nat Nanotechnol* 6(7): 439–445.
22. Kim KS, et al. (2009) Large-scale pattern growth of graphene films for stretchable transparent electrodes. *Nature* 457(7230):706–710.
23. Smith RK, Lewis PA, Weiss PS (2004) Patterning self-assembled monolayers. *Prog Surf Sci* 75(1-2):1–68.
24. Jiang X, Ferrigno R, Mrksich M, Whitesides GM (2003) Electrochemical desorption of self-assembled monolayers noninvasively releases patterned cells from geometrical confinements. *J Am Chem Soc* 125(9):2366–2367.
25. Zhang Y, Salaita K, Lim J, Mirkin CA (2002) Electrochemical whittling of organic nanostructures. *Nano Lett* 2(12):1389–1392.
26. Jang JW, Maspoch D, Fujigaya T, Mirkin CA (2007) A "molecular eraser" for dip-pen nanolithography. *Small* 3(4):600–605.
27. Jang JW, et al. (2008) Electrically biased nanolithography with KOH-coated AFM tips. *Nano Lett* 8(5):1451–1455.
28. Zhang Y, Salaita K, Lim JH, Lee KB, Mirkin CA (2004) A massively parallel electrochemical approach to the miniaturization of organic micro- and nanostructures on surfaces. *Langmuir* 20(3):962–968.
29. Morton SL, Degertekin FL, Khuri-Yakub BT (1998) In situ ultrasonic measurement of photoresist glass transition temperature. *Appl Phys Lett* 72(19):2457–2459.
30. Shao Q, Liu G, Teweldebrhan D, Balandin AA (1992) High-temperature quenching of electrical resistance in graphene interconnects. *Appl Phys Lett* 92(20):202108.
31. Filleter T, et al. (2009) Friction and dissipation in epitaxial graphene films. *Phys Rev Lett* 102(8):086102.
32. Varenberg M, Etsion I, Halperin G (2003) An improved wedge calibration method for lateral force in atomic force microscopy. *Rev Adv Mater Sci* 74(7):3362–3367.
33. Schwarz U (1996) Quantitative analysis of lateral force microscopy experiments. *Rev Sci Instrum* 67(7):2560–2567.
34. Bhushan B, Sundararajan S (1998) Micro/nanoscale friction and wear mechanisms of thin films using atomic force and friction force microscopy. *Acta Mater* 46(11): 3793–3804.